sustainability

MDPI

Article

Comparative Modeling of Greening Design Scenarios for Sustainable and Climate-Responsive Urban Regeneration: Microclimate and Thermal Comfort Effects in an Italian Case Study

Zixin Zhao, Alberto Barbaresi *, Laura Caggiu, Patrizia Tassinari and Daniele Torreggiani

Department of Agricultural and Food Sciences, University of Bologna, Viale Giuseppe Fanin, 48, 40127 Bologna, Italy; zixin.zhao2@unibo.it (Z.Z.); laura.caggiu2@unibo.it (L.C.); patrizia.tassinari@unibo.it (P.T.); daniele.torreggiani@unibo.it (D.T.)

* Correspondence: alberto.barbaresi@unibo.it; Tel.: +39-051-2096197

Abstract

Urban overheating poses major challenges in Mediterranean cities, affecting public health and well-being. This study comparatively evaluates how alternative greening configurations influence urban microclimate and outdoor thermal comfort in a brownfield regeneration site in Imola, Italy, using ENVI-met simulations under a representative extreme summer condition. Eight scenarios with varying vegetation density, structure, and spatial arrangement were modelled on the hottest day of the year, and the Physiological Equivalent Temperature (PET) was evaluated at representative times. Results show that greening reduces heat stress, though its effectiveness varies over time and across configurations. No meaningful cooling occurred at 5:00 a.m., confirming that vegetation has a limited impact during nocturnal radiative processes. At 9:00 a.m., the medium-density scenario (S2b) achieved the greatest PET reduction (~2 °C), suggesting favorable evapotranspiration conditions under moderate radiation. At 4:00 p.m., the distributed high-density scenario (S3.2b) provided the strongest mitigation (~1.8–2 °C). Distributed layouts outperformed clustered ones, highlighting the non-linear nature of vegetation cooling. Zonal analysis showed the largest cooling in public green areas, followed by parking, building, and path zones, demonstrating the influence of surface type and shading geometry. Greening also produced modest improvements in surrounding neighborhoods (up to 0.8 °C in the morning), although impacts remained localized. Overall, results highlight how vegetation quantity, structure, and spatial distribution influence cooling performance under critical summer conditions, supporting climate-responsive urban regeneration design. These findings contribute to sustainable urban planning by supporting nature-based strategies for climate adaptation and improved environmental quality in regenerating urban districts. Future work should consider seasonal vegetation dynamics and multi-objective design optimization.

Keywords: urban microclimate; green infrastructure; sustainable urban regeneration; nature-based solutions; thermal comfort; climate adaptation; human health

Academic Editors: Alejandro Prieto and Elizabeth Wagemann

Received: 31 January 2026
Revised: 7 March 2026
Accepted: 17 March 2026
Published: 22 March 2026

1. Introduction

Global warming and the rapid pace of urbanization are exacerbating climate-related challenges worldwide [1]. Currently, more than half of the global population resides in

urban areas, and this figure is projected to increase to nearly 80% by 2030 [2]. As we know, high building density, limited vegetation, and intensive anthropogenic heat emissions make cities particularly vulnerable to the Urban Heat Island (UHI) phenomenon [3]. The UHI effect, defined as the accumulation of excess heat within urban areas due to low-albedo materials, reduced evapotranspiration, and waste heat generation, can elevate air temperatures by up to 10 °C compared to surrounding rural regions [4].

Urban overheating, compounded by air pollution and extreme weather events, poses serious risks to public health and well-being. During heatwaves, unshaded impervious surfaces such as pavements and rooftops absorb large amounts of solar radiation, intensifying pedestrian heat exposure and increasing the incidence of heat stress, dehydration, and cardiovascular and respiratory disorders [5]. Italy is among the European countries most affected by heat extremes, where elevated temperatures represent one of the leading causes of daily mortality during summer months [6]. In addition to threatening vulnerable populations such as the elderly and children, prolonged heat exposure also reduces outdoor activity levels, undermines mental health, and diminishes the overall livability of cities [5].

In response to these challenges, a growing body of research emphasizes the role of Nature-based Solutions (NbSs), with urban greening being one of the most effective approaches to mitigate urban overheating. Green infrastructure—such as parks, street trees, green roofs, and green walls—enhances evapotranspiration, provides shading, and improves the urban microclimate [7,8]. Recent comparative studies further highlight the thermal potential of rooftop greening systems; for instance, ref. [7] demonstrated that green roofs outperform rooftop greenhouses in reducing surface temperatures and improving hygrothermal performance under Mediterranean climatic conditions, reinforcing the relevance of roof-based greening as a mitigation strategy in Southern Europe. Numerous empirical studies demonstrate their potential: green areas in Lisbon reduced local temperatures by up to 6.9 °C [9], doubling green space in Padova decreased daytime air temperature by 3 °C [10], and green roofs in Berlin lowered the physiological equivalent temperature (PET) by 9 °C [11]. It should be noted that cooling magnitudes reported across different cities, climatic contexts, spatial scales, and thermal indices are not directly comparable. These figures are cited to illustrate the documented relevance of urban greening strategies rather than to establish transferable quantitative benchmarks. Moreover, the thermal performance of greening strategies has been shown to depend on factors such as vegetation type, canopy density, and spatial configuration [6,12].

Although these studies confirm the cooling potential of greening interventions, their effectiveness is highly context-dependent, influenced by plant characteristics, spatial distribution, and the integration within the existing built environment. Systematic assessments of different design configurations and their combined effects are still limited, particularly in urban regeneration contexts. However, there remains a need for structured comparative assessments that systematically examine how variations in vegetation density and spatial configuration influence microclimatic performance within specific urban regeneration contexts. Rather than providing universally transferable solutions, such analyses can clarify context-sensitive design implications under defined climatic conditions.

Additionally, greening strategies are increasingly framed within broader urban planning and architectural debates [13]. European urbanism has long recognized open spaces and environmental infrastructures as structuring elements of contemporary cities [14,15], while more recent perspectives have emphasized the integration of ecological processes and technological performance within urban forms [16,17]. Within this context, simulation-based tools can be understood not only as assessment methods, but also as instruments supporting climate-responsive urban regeneration.

This research aims to fill these gaps by systematically evaluating the effects of alternative greening design options—in terms of vegetation type, proportion, and spatial arrangement—on urban microclimate and human thermal comfort. The analysis is conducted through modeling and simulation approaches applied to a real urban regeneration case study in Italy, where a built-up configuration was established by the municipality and considered a fixed element in this research, which focused on public and private green areas design. By integrating quantitative evaluation with a systematic design framework, this study seeks to identify optimized greening scenarios capable of enhancing thermal comfort, reducing urban overheating, and improving environmental quality. The findings are expected to provide transferable criteria for sustainable urban regeneration, supporting decision-makers and planners in developing resilient, climate-responsive cities.

2. Materials and Methods

This study employed a modelling-based approach to evaluate the microclimatic and thermal comfort performance of alternative greening configurations in an urban regeneration context. The methodological workflow consisted of four main components: (1) definition and characterization of the study area, including local climate, land-use structure, and existing vegetation conditions; (2) development of the input datasets required for ENVI-met, covering buildings, soil, vegetation, and meteorological data; (3) construction and initialization of the ENVI-met model domain, followed by the simulation of nine scenarios representing different levels of vegetation coverage and spatial configurations; (4) post-processing and evaluation of microclimatic and thermal comfort outputs, with a specific focus on the Physiological Equivalent Temperature (PET).

A combination of ENVI-met modules was used to support this workflow. The Spaces module was adopted for 3D model construction and vegetation parametrization, ENVI-guide for meteorological forcing, ENVI-core for microclimatic simulations, and BIO-met for thermal comfort assessment. Model outputs were further processed using Leonardo for spatial visualization and QGIS (Version 3.34.6, QGIS Development Team) for zonal statistical analysis. This integrated approach enabled a multi-scalar examination of vegetation effects—ranging from site-level cooling performance to spillover impacts on adjacent urban areas.

2.1. The Study Area

The study was conducted in the city of Imola, located in the Metropolitan City of Bologna, within the Emilia-Romagna region of northern Italy (Figure 1). Imola is a medium-sized city covering about 204 km^2 with a population of approximately 70,000 inhabitants as of 2023. The local climate is classified as humid subtropical (Cfa) according to the Köppen–Geiger classification [18]. Based on climate normals for the period 1991–2020 [19], the average air temperature is approximately 25 °C in July and about 3 °C in January, while summer conditions are characterized by hot and humid weather with peak temperatures reaching up to 39 °C [7].

The selected study area is situated in the northern part of the city, close to the urban core. The layout of the area is governed by Variant 3 of the Detailed Plan of public initiative N8 Nord Ferrovia of the Municipality of Imola, in force from 28 February 2024. It represents the main area of urban regeneration of the city of Imola, which from a long-disused production and service area is projected towards a future eco-district equipped with greenery and quality urban services. The variant represents the definitive arrangement of the lots, grouped into large courtyards crossed by a single public park and a cycle/pedestrian path. At the western end of the neighbourhood, next to the existing wooded area, a social residential housing complex is planned to be built. It was chosen because its land-use mix,

environmental vulnerabilities, and redevelopment challenges are representative of similar contexts both nationally and internationally.

Figure 1. Location of the study site within Imola, Emilia-Romagna region (Italy).

The study area covers approximately 18.1 ha, comprising three main components: (1) a central brownfield previously used for industrial and logistics functions (food processing and railway maintenance), now abandoned and partially re-vegetated through spontaneous plant growth; (2) an urban forest in the north-western part, forming part of the city's existing green infrastructure; (3) an abandoned agricultural parcel on the eastern side. The area is bounded by a railway to the south (adjacent to dense residential fabric), industrial and commercial zones to the north, sports and agricultural areas to the west, and mixed residential–agricultural areas to the east (Figure 2). As shown in this figure, the ENVI-met computational domain (red boundary) extends beyond the regeneration area (green boundary) in order to evaluate potential microclimatic spillover effects on adjacent urban zones and to provide adequate buffer space for boundary condition stabilization. The extension distances are not uniform, as the domain was shaped to include representative surrounding built areas while minimizing artificial edge effects in the simulation.

The area is included in a municipal regeneration masterplan aimed at promoting resilient urban development through green infrastructure and soft mobility integration, to improve citizens' health and well-being. The development includes buildings and infrastructure whose configuration was established by the municipality and considered a fixed element in this research. Within this framework, the masterplan allocates extensive public and private green areas, whose detailed design, layout, and vegetation composition have been the focus of this research, aimed at testing and optimizing the greening strategies through modeling and simulation (Figure 3).

Figure 2. Model extension showing the regeneration site and the surrounding neighborhoods: (1) central brownfield area; (2) urban forest in the north-western part; (3) abandoned agricultural parcel on the eastern side.

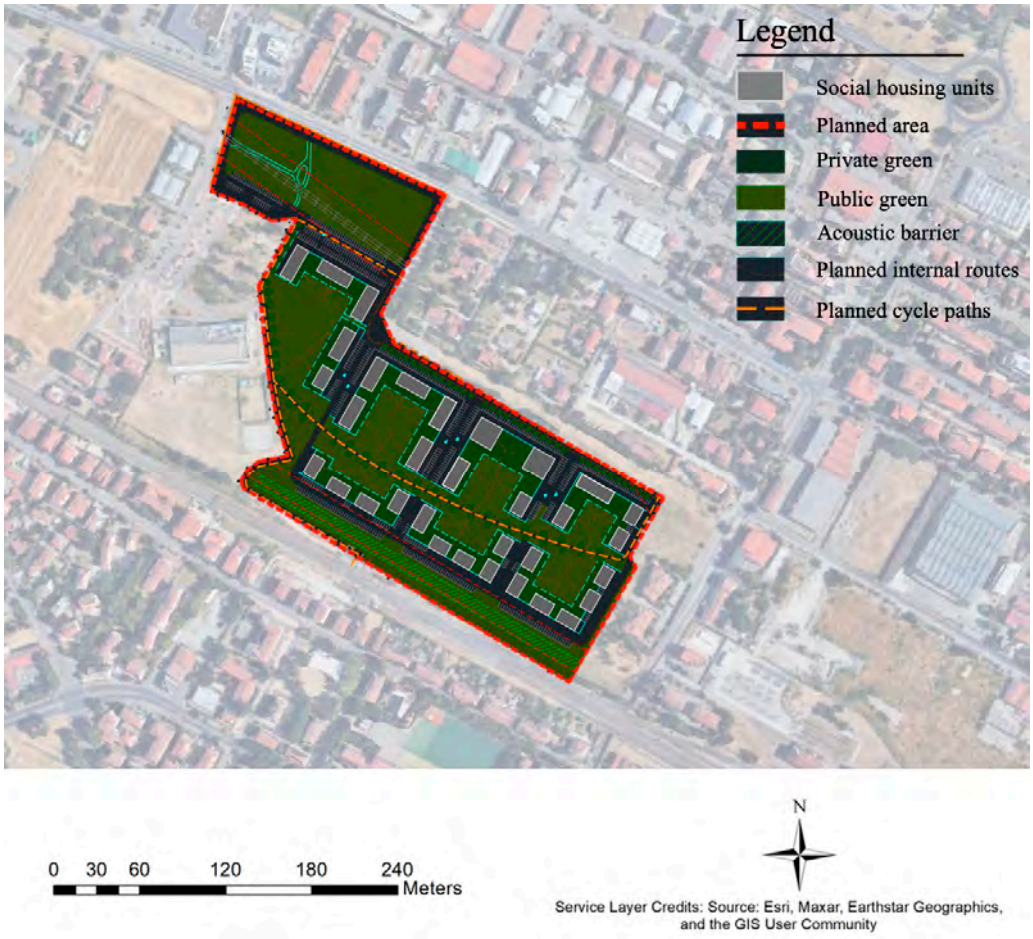

Figure 3. Regeneration masterplan of the study site as defined by Imola Municipality in the Detailed Plan of public initiative N8. The dashed red line indicates the study area boundary, and the dashed lines represent auxiliary boundaries from the source dataset. Colors denote different planned land-use elements.

According to the municipal plan [20], redevelopment will include 33 social housing units arranged in four courtyard blocks, a public parking lot in the northeast, and an internal network of pedestrian and cycle paths connecting residential buildings and facilities. Green areas are planned both publicly and privately—around housing units, along the main and secondary paths, and near parking areas.

This study developed a series of greening design scenarios to quantitatively evaluate and optimize their microclimatic and thermal comfort performance, not only within the regeneration site but also in the surrounding neighborhoods. To capture these broader effects, the model domain was extended to cover an area of 34.8 ha, encompassing both the regeneration zone and its immediate surroundings.

2.2. Input Datasets

The simulations employed four main datasets: vegetation, soil, building, and weather data.

The soil type of Imola is classified as silty clay loam, according to the USDA classification, corresponding to the TEGAGNA and RONCOLE VERDI soil complexes [21].

The vegetation data were obtained from the Imola Municipality and verified through in situ surveys [20]. A georeferenced tree inventory provided by the Municipality enabled detailed mapping and classification of existing vegetation in the north-western park, which forms part of the city's green infrastructure and will be preserved in the regeneration plan.

Table 1 lists the existing tree species and their quantities. The park includes a variety of broadleaf species such as *Acer campestre*, *Fraxinus excelsior*, and *Quercus robur*, representing a structurally diverse composition that contributes to evapotranspiration and canopy shading effects within the study area.

Table 1. Existing tree species and quantities in the north-western park.

Existing Trees	Scientific Name	Count
Pear	*Pyrus communis*	13
Hornbeam	*Carpinus betulus*	7
Ash	*Fraxinus excelsior*	27
Field maple	*Acer campestre*	59
Maple (unspecified species)	*Acer* spp.	8
Oak	*Quercus robur*	86
Black walnut	*Juglans nigra*	1
Wild cherry	*Prunus avium*	3
Holm oak	*Quercus ilex*	9
Lombardy poplar	*Populus nigra* var. *italica*	2
Total		215

The building dataset was generated using Google Earth Pro (version 7.3). Two-dimensional satellite imagery was used to measure building footprints, while heights were derived from the number of floors identified through Street View analysis and on-site surveys. Most residential buildings in the study area are characterized by red-tiled roofs, whereas roofs in the commercial areas are light gray. The geometric and material parameters thus collected were used to model the building layer.

The meteorological data were obtained from the nearest weather station, located 3.07 km from the study site. This station was selected because its surrounding urban morphology—population density, built-up structure, and vegetation ratio—closely resembles that of the study area. Other available stations were excluded due to their different environmental contexts: one situated 6.88 km away in a mountainous zone with dense tree cover, and another 11.22 km away in a rural area dominated by farmland and scattered

buildings. Hourly data for air temperature (Ta), relative humidity (RH), wind speed, and prevailing wind direction were collected for the entire year 2023 to define the boundary conditions for simulations.

2.3. Modelling Framework

The simulations were performed using the ENVI-met software (Version 5, ENVI-met GmbH, Essen, Germany), which is a three-dimensional, non-hydrostatic microclimate model based on the principles of thermodynamics and fluid dynamics [22]. ENVI-met enables the simulation of complex interactions among buildings, vegetation, soil, and atmosphere at high spatial and temporal resolutions. It includes submodules for model initialization and boundary condition definition, vegetation growth and transpiration, soil and surface energy balance, and building heat exchange [23]. Numerous studies have validated its accuracy in reproducing urban microclimatic conditions and assessing the effectiveness of greening strategies for heat mitigation [24].

Both the *ex-ante* (pre-regeneration) and green mitigation scenarios were modeled in the *Spaces* module of ENVI-met, which was used to define the geometric configuration of buildings, vegetation, and surfaces (Figure 4). Meteorological inputs corresponding to the selected day were processed in *ENVI-guide*. The main computational processes were then executed in *ENVI-core*, where the model solved the coupled equations for air temperature, humidity, wind flow, and radiation fluxes across the study domain.

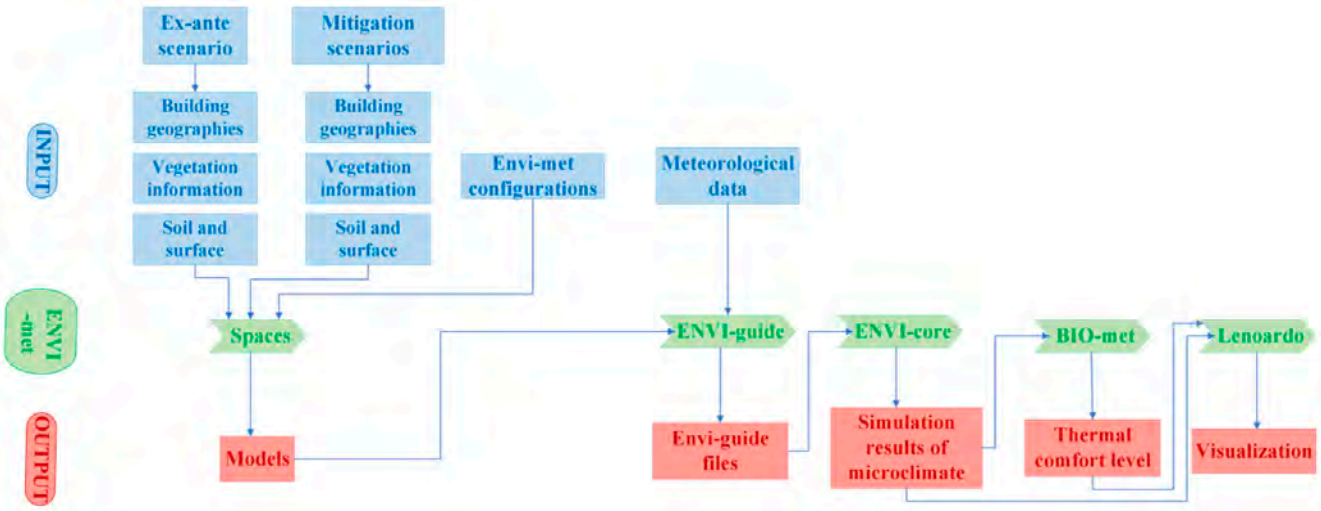

Figure 4. Framework of the ENVI-met simulation process and existing vegetation distribution.

Human thermal comfort was evaluated using the *BIO-met* module, which integrates meteorological outputs from ENVI-core to calculate several comfort indices, including PET, UTCI, SET, and PMV/PPD. Among these, the Physiological Equivalent Temperature (PET) was selected as the key indicator, as it provides a direct link between outdoor thermal conditions and human thermal perception.

Spatial visualization and post-processing were conducted using Leonardo (Version 5.x, ENVI-met GmbH, Germany), the official visualization and analysis module integrated within ENVI-met v5. Leonardo was used to generate horizontal and vertical cross-sectional maps of air temperature, PET, wind speed, and mean radiant temperature (Tmrt), as well as three-dimensional visualizations of vegetation and building configurations (Figure 5).

Scenario	Vegetation cover	3D model
Ex-ante	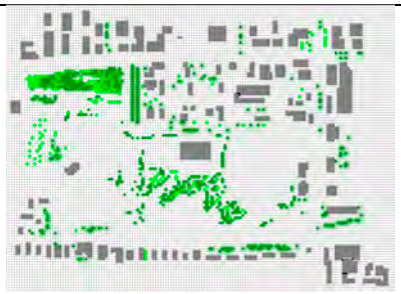	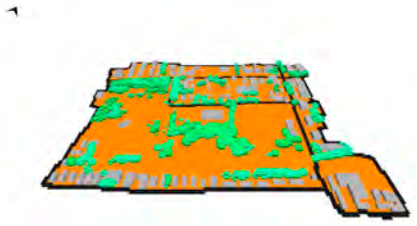
S1a		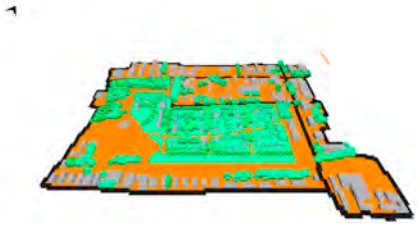
S1b	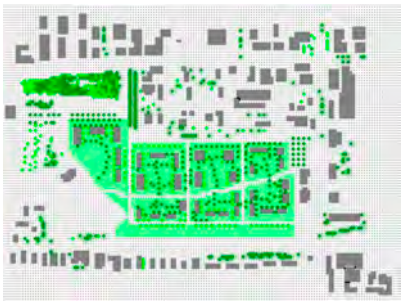	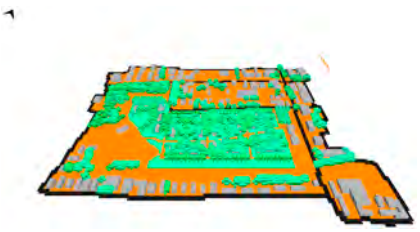
S2a		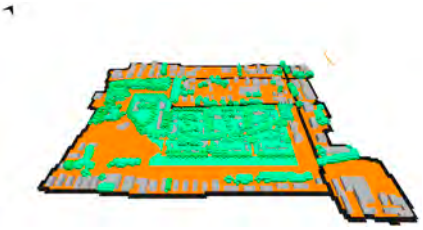
S2b		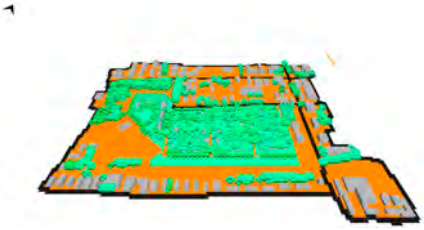

Figure 5. *Cont.*

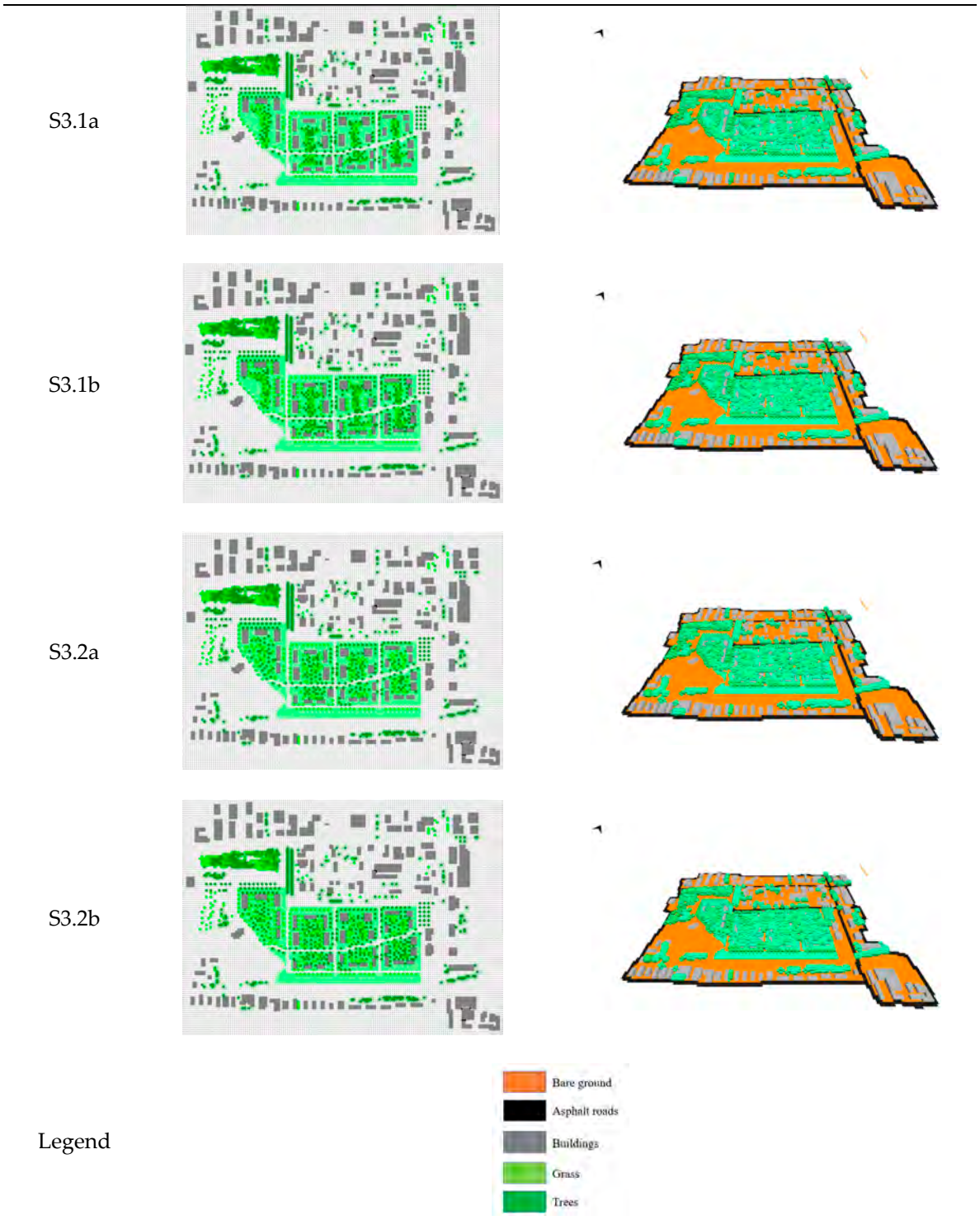

Figure 5. Three-dimensional ENVI-met model and vegetation cover for the regeneration area.

Raster outputs were then exported from Leonardo in ASCII format and further processed in QGIS 3.34.6 for zonal statistics, spatial classification, and comparative analysis across land-use types. While QGIS was employed for statistical aggregation and cartographic refinement (Figures below), Leonardo was specifically used for ENVI-met-native data interpretation and 3D model visualization.

ENVI-met v5 (including the Leonardo module) has been widely applied in urban microclimate studies [22,24].

A spatial classification and statistical analysis of the processed results were performed using QGIS 3.34.6. As a final step, PET variation across distinct functional zones and adjacent urban contexts was quantified as part of the post-simulation evaluation, which enabled a more comprehensive understanding of spatial heterogeneity and the effectiveness of the proposed greening interventions in cooling localized environments.

2.4. Model Initialization and Configuration

Before starting the simulation, ENVI-met was configured for model size selection, grid cell size, and study area location. To facilitate modeling, the original site geometry was rotated by −28° to better align the urban layout with the orthogonal ENVI-met grid geometry, thereby improving the geometric representation of buildings and surfaces within the computational domain [22,25]. This rotation does not alter the spatial extent or resolution of the analyzed raster data.

Because ENVI-met defines wind direction relative to the model grid, the prevailing wind direction was rotated consistently by the same angle to preserve the correct physical relationship between airflow patterns and urban morphology. This ensures coherence between site orientation and meteorological forcing and avoids artificial distortion of wind–building interactions.

Other ENVI-met configurations and initializations are presented in Table 2.

Table 2. ENVI-met model configuration and initialization parameters.

Parameters	Parameter Specification	Study Setting
Model Location	Name of location	Imola, Emilia-Romagna region, Italy
	Latitude	44°36′ N
	Longitude	11°71′ E
	Reference Time Zone	CEST (UTC + 2)
Model geometry	x-Grids	173
	y-Grids	135
	z-Grids	25
Size of grid cell (m)	dx	5
	dy	5
	dz	2
	Model rotation out of the grid north	−28

The computational domain consisted of 173 × 135 × 25 grid cells with a horizontal resolution of 5 m × 5 m and a vertical resolution of 2 m for the lowest layer. This corresponds to an approximate horizontal extent of 865 m × 675 m. Domain dimensions and grid resolutions are consistent with commonly adopted configurations in ENVI-met neighborhood-scale simulations [24,25]. The domain includes peripheral buffer zones surrounding the 18.1 ha core study area; specifically, five empty grid cells were added in all horizontal directions to minimize artificial boundary effects and to allow wind and thermal fields to develop before interacting with the area of interest. The total model height was set to 50 m, which is approximately twice the height of the tallest building in the study area (25 m), ensuring sufficient vertical space to capture rooftop-level flow and boundary-layer adjustment processes. Similar vertical extents have been demonstrated to adequately capture near-surface boundary-layer adjustment in comparable urban microclimate studies [25].

Hourly time-series data of air temperature, relative humidity, wind speed, and prevailing wind direction for 18 July were input into ENVI-guide as boundary conditions using the simple forcing option. Incoming radiation and cloud forcing were implemented using the ENVI-met default radiation parameterization based on available meteorological

information. This radiation scheme follows the standard ENVI-met solar geometry and atmospheric transmissivity formulation described in [22]. All simulation times refer to local summer time in Italy (Central European Summer Time, CEST; UTC + 2). The simulation day (18 July) and the selected time points (05:00, 09:00, and 16:00) were identified based on heat index analysis to represent low, intermediate, and peak thermal stress conditions, allowing the evaluation of greening performance under representative extreme summer conditions.

Thermophysical parameters of ground and building surfaces—including albedo, emissivity, thermal conductivity, volumetric heat capacity, and surface roughness—were assigned using the default ENVI-met material library and adjusted where site-specific information was available. Initial soil moisture was set to default dry-summer baseline conditions, and irrigation was not explicitly considered in order to assess the cooling performance of greening strategies without artificially enhanced evapotranspiration in line with low-water-input green design commonly used in public spaces to increase their sustainability. Vegetation properties, including plant height, crown dimensions, LAI/LAD, and stomatal resistance, were assigned using ENVI-met plant templates to represent typical urban vegetation types observed in the study area and to ensure consistent comparison across greening scenarios.

2.5. Green Design Scenarios

In the study area, the lengths of the four main planned roads running north–south and distributed in the four "courtyards" are 130 m, 220 m, 150 m, and 190 m, respectively. The length of the secondary planned road running east–west is 520 m. The geometric dimensions of the 33 planned housing units in the study area are shown in Table 3. The area within 6 m from the buildings is allocated to private greening, and the part exceeding 6 m is planned for public greening. Parking lots are set up in the south of the urban forest, on the east side of the residential area, and near each building, with a total area of 23,100 square meters.

Table 3. Geometric dimensions of the planned housing units.

Length	Width	Floors	Quantity	Remark
32	12	4	3	shu1–shu3
30	12	4	6	shu4, shu6–shu9, shu16
20	12	3	7	shu5, shu10–shu13, shu17, shu24
22	22	4	2	shu14–shu15
24	12	3	1	shu18
18	12	2	8	shu19–shu22, shu25–shu26, shu31–shu33
34	12	4	1	shu23
20	12	2	4	shu27–shu30

The landscape design approach used in this study to generate the greening scenarios aims to create a green residential complex that is ornamental, livable, diverse, and comfortable for people's well-being. In terms of public greening, lawns have been designed in all public green spaces, and then the number and type of trees are designed according to the context and space conditions. In this study, in areas with ample space, such as on both sides of the main roads, large trees are used to shade pedestrians and roads, increase evapotranspiration, and help to cool the city. In areas with limited space, such as secondary roads, parking lots, and private green areas, smaller trees are used to balance the space for pedestrians and greenery.

Plant selection is based on allocating 20–25% to first-size trees, 25–35% to second-size trees, and 40–45% to third-size trees, and species proportions were maintained equal within

each tree size category to ensure consistency in canopy structure and leaf area density across scenarios [26].

Rationale for Plant Selection

The selection of tree species was guided by ecological coherence, spatial-functional suitability, climatic adaptability, and modelling reliability. Species already present within the study area—such as *Fraxinus excelsior*, *Acer campestre*, and *Carpinus betulus*—were prioritized to maintain ecological continuity and landscape identity. Extending locally adapted species contributes to long-term resilience and supports biodiversity integration within urban regeneration projects.

Tree size categories were defined according to canopy height and spatial function within the masterplan layout. Large-canopy species were allocated along primary pedestrian corridors and open public spaces to maximize shading and evapotranspiration, which are recognized as key mechanisms for urban heat mitigation [27,28]. Medium- and small-canopy species were introduced in secondary paths, parking areas, and private green spaces where spatial constraints limit canopy expansion but localized shading remains beneficial.

Species selection also considered physiological suitability for Mediterranean climatic conditions, including drought tolerance, resistance to pests, and adaptability to compacted urban soils. These traits are particularly relevant under increasing summer temperature extremes and prolonged dry periods projected for Southern Europe [4,5].

To ensure parameter consistency, numerical stability, and reproducibility within the ENVI-met environment, tree species were selected from the validated ENVI-met v5 plant database. The use of predefined plant templates minimizes uncertainties associated with user-defined parameterization and ensures compatibility with the model's physiological and aerodynamic submodules [22,24].

According to the configuration of the greening scenarios, this study follows an incremental design principle. Starting from a minimal tree coverage, the proportion of trees was progressively increased to quantify the contribution of vegetation structure—rather than total green area—to the local microclimate and outdoor thermal comfort. To further distinguish the respective influence of public and private green spaces, each scenario was divided into two sub-scenarios: type A considers only public greenery, while type B integrates both public and private green areas. Tree numbers were calculated based on spacing and spatial availability under each design condition.

Eight vegetation scenarios (S1a–S3.2b) were developed following this principle, representing a progressive enhancement of tree quantity and structural complexity. The configurations range from the simplest turf-dominated layout to multi-layered urban forest systems integrating trees of different sizes and spatial arrangements (Table 4).

Table 4. Size and species of trees used for mitigation measures.

1st Size Trees	2nd Size Trees	3rd Size Trees
Fraxinus excelsior	*Acer campestre*	*Albizia julibrissin*
Tilia spp.	*Carpinus* spp.	*Koelreuteria paniculata*
Aesculus hippocastanum	*Fraxinus* spp.	*Jacaranda mimosifolia*

S1a represents the baseline configuration, featuring the lowest tree coverage. Turf was applied to all open areas, while first-size trees (*Fraxinus excelsior*, *Tilia* spp., *Aesculus hippocastanum*) were planted along the west sides of the four main pedestrian paths to provide shading in summer. Based on the total path lengths (130 m, 220 m, 150 m, and 190 m) and a 10 m planting interval [26], a total of 69 large trees were allocated, evenly distributed among the three species. Second-size trees (*Acer campestre*, *Carpinus betulus*,

Fraxinus spp.) were planted in parking areas—one tree every two parking spaces—for a total of 165 trees. Hedges were set between public and private green zones to define spatial boundaries and enhance privacy.

S1b extends S1a by introducing private greening around residential buildings. Given the limited area and building height, a mix of medium- and small-size trees was adopted, including 34 s-size trees (*Acer campestre*, *Carpinus betulus*, *Fraxinus* spp.) and 96 third-size trees (*Albizia julibrissin*, *Koelreuteria paniculata*, *Jacaranda mimosifolia*).

S2a increases the proportion of public greenery and introduces second-size trees along the secondary paths (345 m in total), planting 52 trees evenly distributed across *Acer campestre*, *Carpinus betulus* and *Fraxinus* spp. S2b builds upon S2a by adding private greening consistent with the S1b configuration.

S3.1a and S3.1b represent cluster-based planting strategies. Additional medium- and small-size trees (72 and 135, respectively) were grouped along main paths to form neighborhood-scale urban forest clusters. In contrast, S3.2a and S3.2b apply the same number and species of trees but adopt a distributed layout, evenly spreading vegetation throughout public spaces to enhance overall microclimatic balance.

This hierarchical and progressive vegetation framework—from turf-based configurations to structurally diverse multi-layered greenery—enabled a systematic assessment of how tree density, spatial distribution, and structural composition influence the outdoor thermal environment and pedestrian comfort.

The elaboration, plant species, and number of plants in each scenario are shown in Table 5 and Figure 5 show a three-dimensional model of the entire study area and the vegetation cover of the regeneration area.

Table 5. Vegetation configuration and tree species in the greening scenarios.

Scenarios	Vegetation Recipes	Total Numbers	Species	Numbers
S1a	Turf			
	1st size trees along main paths	69	*Fraxinus excelsior* *Tilia cordata* *Aesculus hippocastanum*	23-23-23
	2nd size trees in parking areas	165	*Acer campestre* *Carpinus betulus* *Fraxinus*	55-55-55
	Hedges between public and private green areas			
S1b	S1a			
	2nd size trees in private areas	34	*Acer campestre* *Carpinus betulus* *Fraxinus*	12-11-11
	3rd size trees in private areas	96	*Albizia julibrissin* *Koelereuteria paniculata* *Jacaranda mimosifolia*	32-32-32
S2a	S1a			
	2nd size along secondary paths	52	*Acer campestre* *Carpinus betulus* *Fraxinus*	17-17-18
S2b	S1b			
	2nd size along secondary paths	52	*Acer campestre* *Carpinus betulus* *Fraxinus*	17-17-18

Table 5. *Cont.*

Scenarios	Vegetation Recipes	Total Numbers	Species	Numbers
S3.1a	S2a			
	Urban forests clustered along main paths in each neighborhood using 2nd size trees	72	*Acer campestre* *Carpinus betulus* *Fraxinus*	24-24-24
	Urban forests clustered along main paths in each neighborhood using 3rd size trees	135	*Albizia julibrissin* *Koelereuteria paniculata* *Jacaranda mimosifolia*	45-45-45
S3.1b	S2b			
	Urban forests clustered along main paths in each neighborhood using 2nd size trees	72	*Acer campestre* *Carpinus betulus* *Fraxinus*	24-24-24
	Urban forests clustered along main paths in each neighborhood using 3rd size trees	135	*Albizia julibrissin* *Koelereuteria paniculata* *Jacaranda mimosifolia*	45-45-45
S3.2a	S2a			
	Distributed trees around buildings using 2nd size trees	72	*Acer campestre* *Carpinus betulus* *Fraxinus*	24-24-24
	Distributed trees around buildings using 3rd size trees	135	*Albizia julibrissin* *Koelereuteria paniculata* *Jacaranda mimosifolia*	45-45-45
S3.2b	S2b			
	Distributed trees around buildings using 2nd size trees	72	*Acer campestre* *Carpinus betulus* *Fraxinus*	24-24-24
	Distributed trees around buildings using 3rd size trees	135	*Albizia julibrissin* *Koelereuteria paniculata* *Jacaranda mimosifolia*	45-45-45

Vegetation structural and physiological parameters, including tree height, crown diameter, root depth, leaf area index (LAI), leaf area density (LAD) profile, and stomatal resistance, were explicitly defined for all species used in the ENVI-met simulations. Parameter values were adopted from the ENVI-met v5 plant database and cross-checked with published studies on Mediterranean urban tree species [22,24,28]. The complete set of structural and physiological parameters assigned to each tree species is summarized in Table 6.

Table 6. Structural and physiological parameters of tree species used in ENVI-met simulations.

Species	Height (m)	Crown Diameter (m)	Root Depth (m)	LAI	Stomatal Resistance (s m^{-1})	LAD Profile
1st size trees						
Fraxinus excelsior	20	12	1.2	4.5	150	Default deciduous vertical distribution
Tilia spp.	18	14	2	5	180	Default deciduous vertical distribution
Aesculus hippocastanum	18	12	2.5	4	160	Default deciduous vertical distribution
2nd size trees						
Acer campestre	14	9	3	3.5	200	Default deciduous vertical distribution
Carpinus betulus	14	9	5	3.8	220	Default deciduous vertical distribution
Fraxinus spp.	15	10	2	4.2	170	Default deciduous vertical distribution
3rd size trees						
Albizia julibrissin	11	8	2	3	250	Sparse vertical canopy distribution
Koelreuteria paniculata	10	8	2	3	240	Sparse vertical canopy distribution
Jacaranda mimosifolia	12	9	2.5	3.8	210	Semi-open canopy vertical distribution

2.6. The Physiological Equivalent Temperature (PET) and the Proposed PET Indices

In the BIO-met module of ENVI-met, several different thermal comfort indices are available [23], such as physiological equivalent temperature (PET), universal thermal climate index (UTCI), Predicted Mean Vote (PMV)/Predicted Percentage Dissatisfied (PDD), etc. The PET index has been proven to be effective in defining human perceived thermal comfort by taking into account various dimensions such as humid and heat conditions, outdoor parameters, human heat exchange, and human metabolism [29]. In this study, 9 simulations were run, and PET was used to analyze the effects of different models on human thermal comfort (Table 7).

Table 7. Human thermal sensation corresponding to PET values [28].

PET (°C)	Thermal Grade of Physiological Perception	Grade of Physiological Perception Stress
<4.0	Very cold	Extreme cold stress
4.1–8.0	Cold	Strong cold stress
8.1–13.0	Cool	Moderate cold stress
13.1–18.0	Slightly cool	Slight cold stress
18.1–23.0	Comfortable	No thermal stress
23.1–29.0	Slightly warm	Slight heat stress
29.1–35.0	Warm	Moderate heat stress
35.1–41.0	Hot	Strong heat stress
>41.1	Very Hot	Extreme heat stress

3. Results and Discussion

The heat index, a formula combining temperature and humidity, has been shown to effectively represent perceived temperature [30]. Calculating the heat index using weather data from the study area throughout the summer of 2023 revealed that 18 July had the highest daily and hourly average heat indexes, occurring at 4 p.m. (Figure 6). The hottest day of the year was therefore selected to represent a worst-case heat-stress scenario for design evaluation, as greening strategies intended for urban regeneration should remain effective under extreme summer conditions. To evaluate the benefits and performance of various greening scenarios and green design strategies under different levels of thermal stress, three representative time points were selected for simulation based on the heat index values. Specifically, the lowest, intermediate, and highest heat index values corresponded to 5:00 a.m., 9:00 a.m., and 4:00 p.m., respectively, capturing key phases of the diurnal thermal cycle (nocturnal cooling, morning warming, and peak afternoon heat stress). While this approach supports design-oriented assessment under critical conditions, future work should extend the analysis to average seasonal and intermediate weather conditions to further test the robustness and transferability of the proposed greening strategies.

The following sections present the simulation results of different greening scenarios at the three selected time points, illustrating the spatial distribution of PET and comparing their cooling performances.

Moreover, to enable a more detailed evaluation of the eight greening scenarios within the study area, the site was further divided into four functional zones based on land-use characteristics: (1) parking area; (2) building area; (3) path area; (4) public green area. For each zone, the PET values were statistically analyzed to quantify and compare the thermal benefits produced by the various greening configurations.

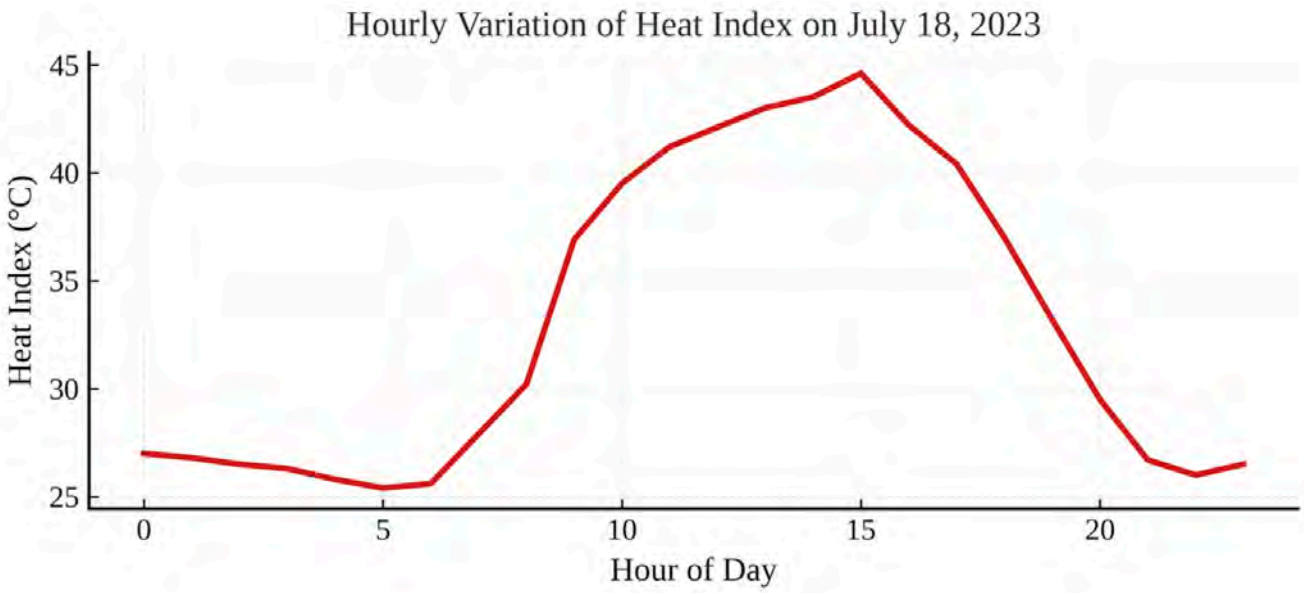

Figure 6. Hourly variation in the heat index on 18 July 2023.

Finally, to investigate the scale of the effect of the greening interventions and their potential broader impacts on the surrounding environment, a comparative statistical analysis was performed to assess how different greening intensities influence thermal comfort not only within the regeneration area but also in its adjacent urban context.

3.1. PET Spatial Distribution Under Different Greening Scenarios

This subsection provides a spatial overview of the Physiological Equivalent Temperature (PET) distribution across different greening scenarios and times of the day. The objective is to visualize how vegetation density and configuration influence the microclimate during early morning, mid-morning, and late afternoon conditions. The results presented in Figure 7 reveal both the magnitude and spatial variability of the cooling effect within the regeneration area.

At 5 a.m., PET values are uniformly low (below 28 °C) across all scenarios. Differences among greening configurations are negligible, and spatial patterns of PET are largely homogeneous.

At 9 a.m., PET values increase significantly, especially in areas with high surface imperviousness. Noticeable cooling effects were observed in scenarios with higher vegetation coverage, particularly around tree-shaded zones and public green areas. The medium-density greening scenario (S2b) achieves the greatest reduction in PET, with average decreases of approximately 2 °C compared to the baseline.

By 4 p.m., PET values reach their daily maximum, exceeding 36 °C over most built-up areas. The distributed high-density greening configuration (S3.2b) provides the strongest mitigation, reducing PET by approximately 1.8–2 °C in vegetated and shaded areas. Distributed layouts exhibit lower PET values than clustered configurations with comparable vegetation density.

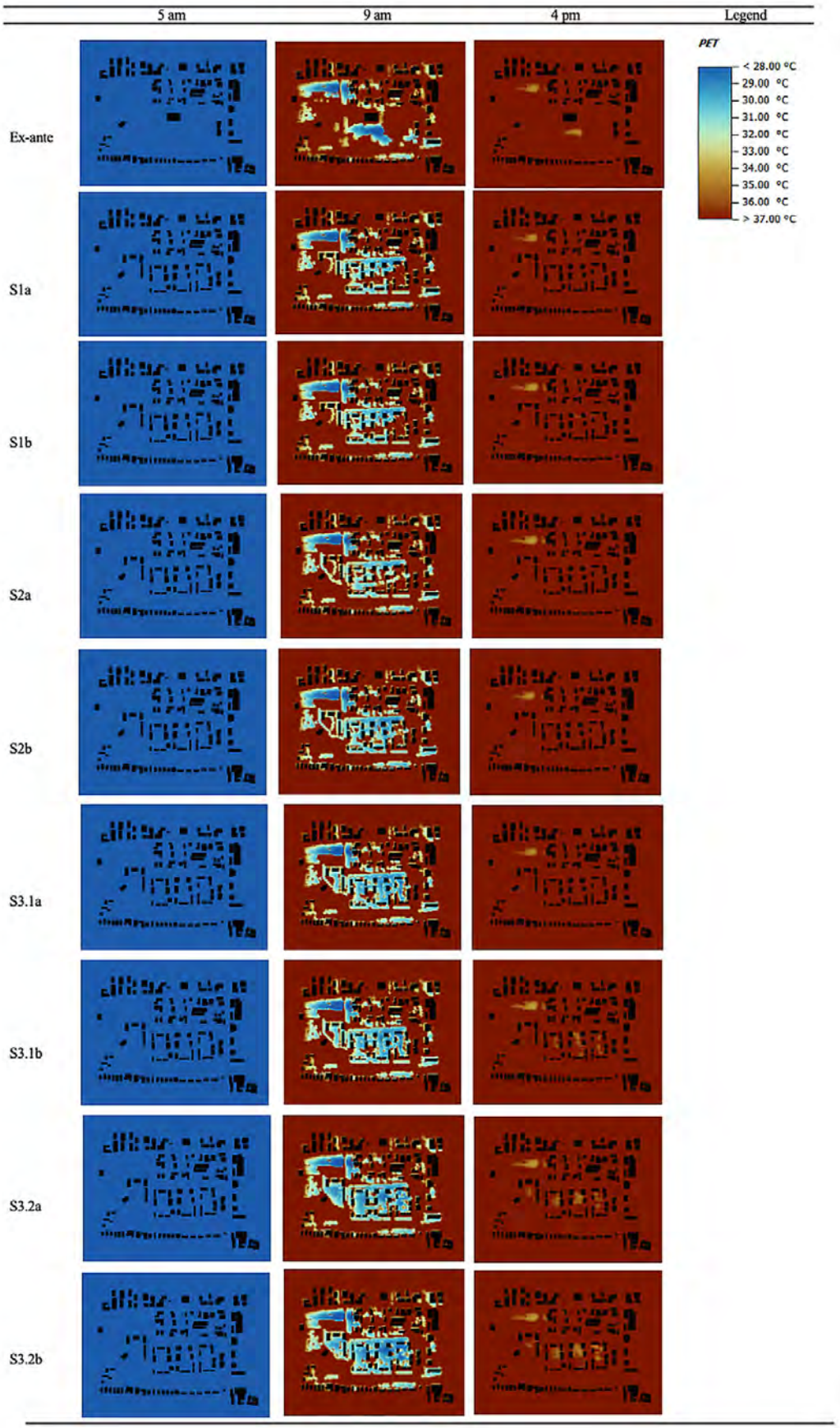

Figure 7. Spatial distribution of PET across baseline and greening scenarios (S1a–S3.2b) at 5 a.m., 9 a.m., and 4 p.m. Black areas indicate building footprints (non-simulated surfaces).

3.2. Zonal PET Analysis

To gain deeper insights into how greening interventions affect specific surface types, this subsection analyzes PET variations within distinct functional zones of the regeneration area, namely building areas, parking areas, path areas, and public green areas. Statistical comparisons across scenarios and time periods (Figures below) enable the evaluation of the relative cooling efficiency of each surface type under varying vegetation configurations.

Zonal Definition and Statistical Procedure

For the zonal statistical analysis, only outdoor open-space grid cells were considered. Building body grids representing enclosed built volumes were excluded to ensure that PET values reflect pedestrian-level outdoor thermal exposure conditions.

The regeneration area was subdivided into four functional zones based on the land-use layout of the masterplan (Figure 8):

(1) Building surroundings: This zone includes open spaces adjacent to building footprints, such as courtyards and paved areas. Building volumes themselves were excluded from the analysis.
(2) Path areas: The path zone was defined using the original planned pedestrian and cycling path geometries. A 5 m buffer was applied on both sides of the centerline to represent the effective pedestrian use area and corresponding thermal exposure corridor.
(3) Parking areas: Parking zones correspond to the designated parking polygons defined in the masterplan layout. These include impervious paved surfaces allocated for vehicle parking and associated circulation spaces.
(4) Public green areas: This zone comprises all designated public green spaces, including lawns and vegetated areas beyond the 6 m private setback from buildings, as defined in the planning scheme.

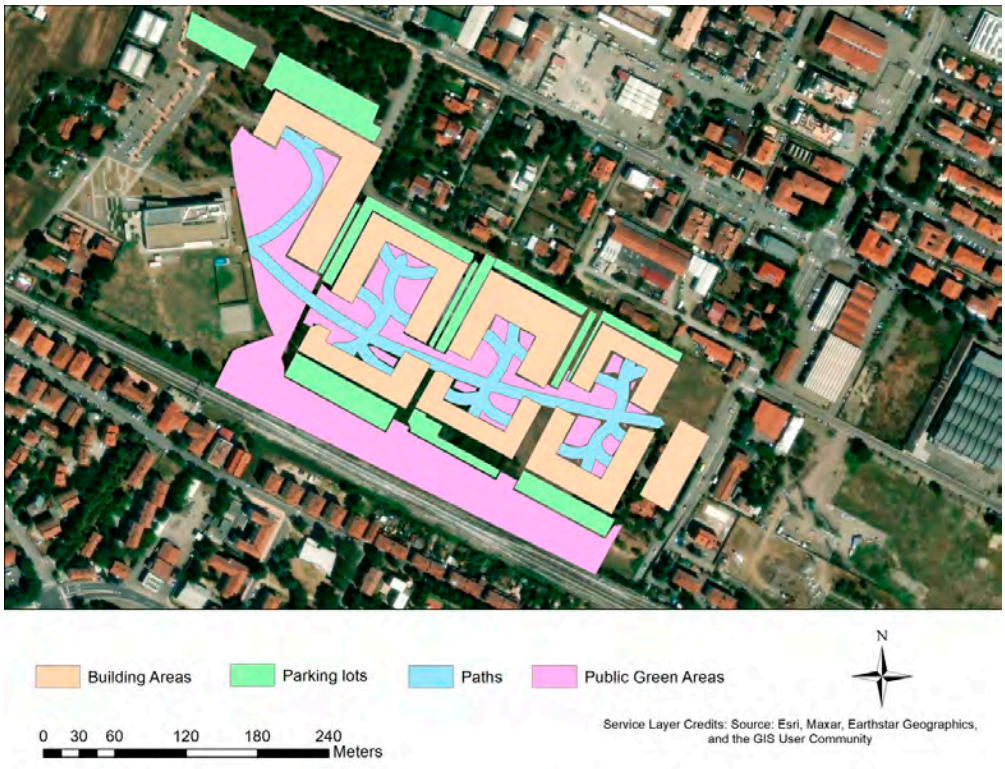

Figure 8. Spatial subdivision of the regeneration area into four functional zones for PET statistical analysis: building area; parking area; path area; public green area.

ENVI-met PET raster outputs at 1.5 m height were imported into QGIS and spatially intersected with these zone polygons. Zonal statistics were calculated using raster cell values. Because all ENVI-met grid cells share identical spatial resolution (5 m × 5 m), zonal mean PET values are implicitly area-weighted.

No additional buffer was applied to building surroundings or parking areas beyond the path-specific buffer described above.

The objective of this zonal analysis was to assess how greening interventions affect different types of frequently used urban spaces, representing distinct patterns of human activity and surface characteristics within the regeneration site.

Figures 9–11 illustrate the distribution of PET values in the different zones at 5 a.m., 9 a.m., and 4 p.m. under all greening scenarios.

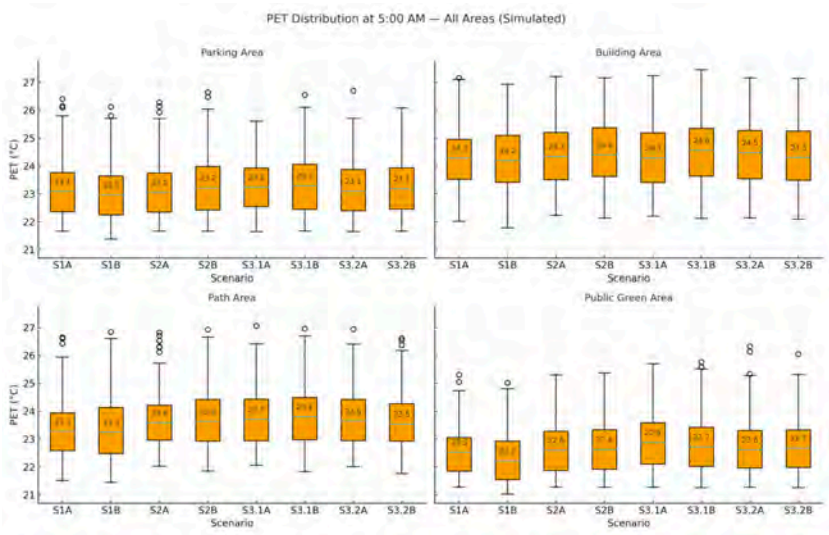

Figure 9. PET distribution at 5:00 a.m. under different greening scenarios for the four functional zones (parking, building, path, and public green areas). Boxplots represent the distribution of PET values, where the box indicates the interquartile range (IQR), the horizontal line inside the box represents the median, whiskers denote the data range, and circles indicate outliers.

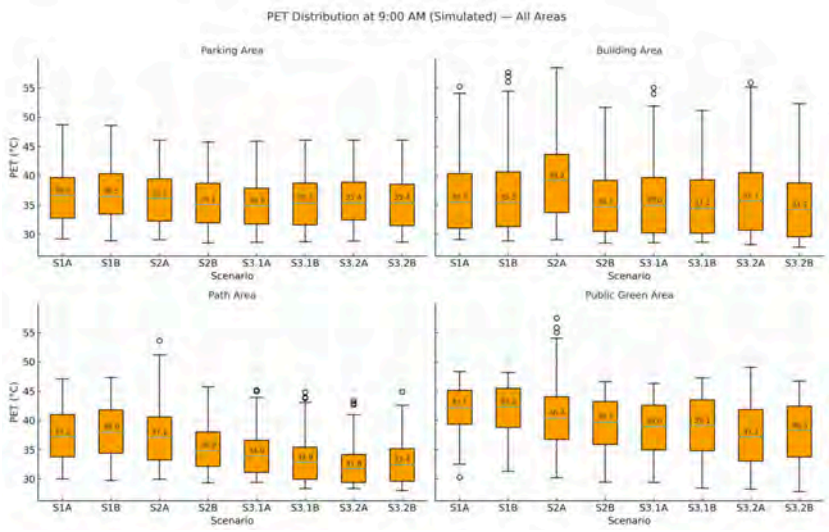

Figure 10. PET distribution at 9:00 a.m. under different greening scenarios for the four functional zones (parking, building, path, and public green areas). Boxplots represent the distribution of PET values, where the box indicates the interquartile range (IQR), the horizontal line inside the box represents the median, whiskers denote the data range, and circles indicate outliers.

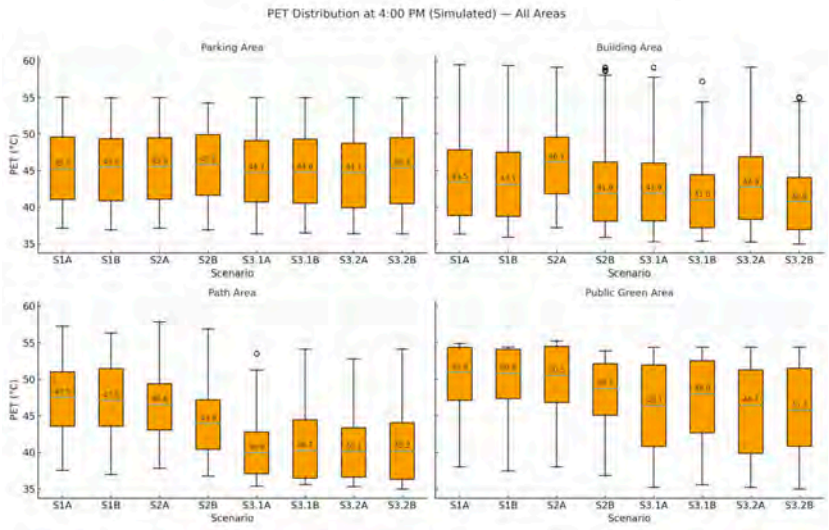

Figure 11. PET distribution at 4:00 p.m. under different greening scenarios for the four functional zones (parking, building, path, and public green areas). Boxplots represent the distribution of PET values, where the box indicates the interquartile range (IQR), the horizontal line inside the box represents the median, whiskers denote the data range, and circles indicate outliers.

Across all scenarios, public green areas consistently show the lowest PET values, followed by parking areas, building surroundings, and path areas.

At 5 a.m., limited temperature variation is observed across scenarios.

At 9 a.m., PET increases sharply across all zones, but greening interventions begin to show clear differentiation. The S2b scenario achieves the greatest PET reduction, especially in the public green and parking areas.

At 4 p.m., all zones experience peak PET values, with the S3.2b distributed greening scenario performing best overall. Compared with the baseline configuration (S1a), PET decreased by up to 2.0–2.5 °C in public green spaces and 1.5–2.0 °C in parking zones.

3.3. Scale of Greening-Intervention Benefits

This subsection investigates the scale of the positive effects of the greening interventions, and in particular aims at understanding if and to what extent the cooling effects of the greening strategies implemented within the regeneration site extend beyond its boundaries into the adjacent urban fabric. To investigate the potential broader impacts of the greening interventions on the thermal comfort of the surrounding environment, a comparative statistical analysis was performed for the *ex ante* condition and multiple greening scenarios. In particular, to quantify this phenomenon in a spatially explicit perspective, the analysis compares PET distributions in two representative surrounding zones, labeled area A and area B (Figure 12), under the baseline, the scenario with the lowest level of greening (S1a), and the two scenarios with the highest greening levels (S3.1b and S3.2b), to assess the extent and intensity of microclimatic spillover effects generated by vegetation.

The effects of the greening strategies on the surrounding areas (A and B) show a time-dependent and spatially limited behavior.

Figure 13 compares PET distributions under the ex-ante condition and the most representative greening scenarios (S1a, S3.1b, and S3.2b). At 9:00 a.m., all mitigation configurations yield moderate decreases in mean PET relative to the ex-ante condition. In Area A, average PET falls from 44.8 °C to approximately 44.2–44.3 °C (reductions of 0.5–0.6 °C), while Area B experiences larger decreases, from 43.8 °C to 42.9–43.2 °C (reductions of 0.6–0.8 °C).

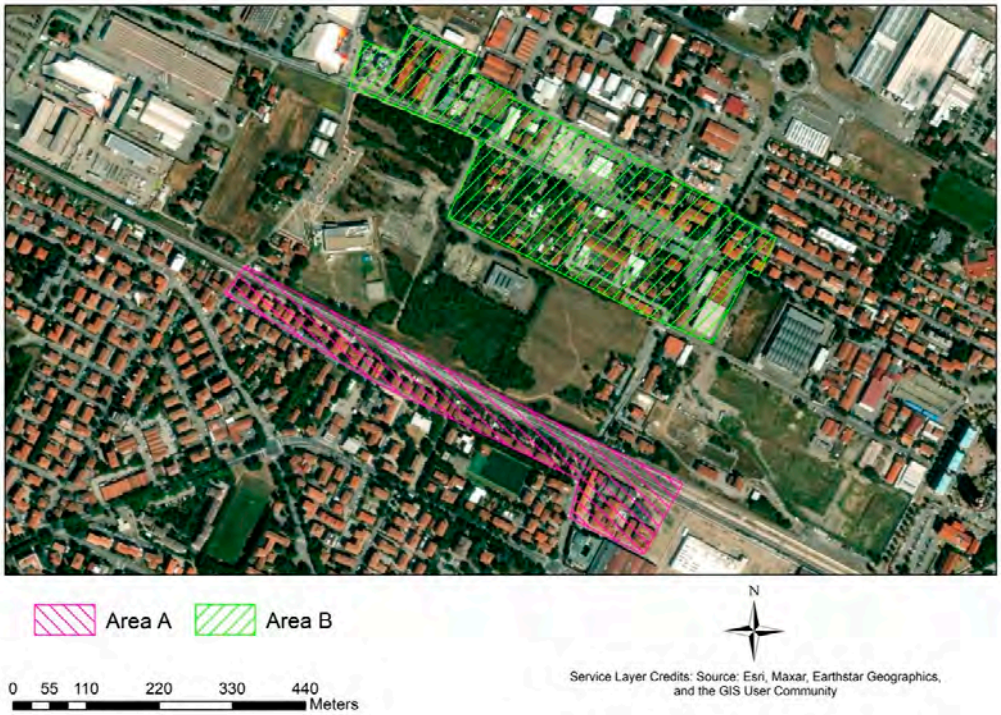

Figure 12. Definition of the surrounding area used for PET analysis under different greening scenarios.

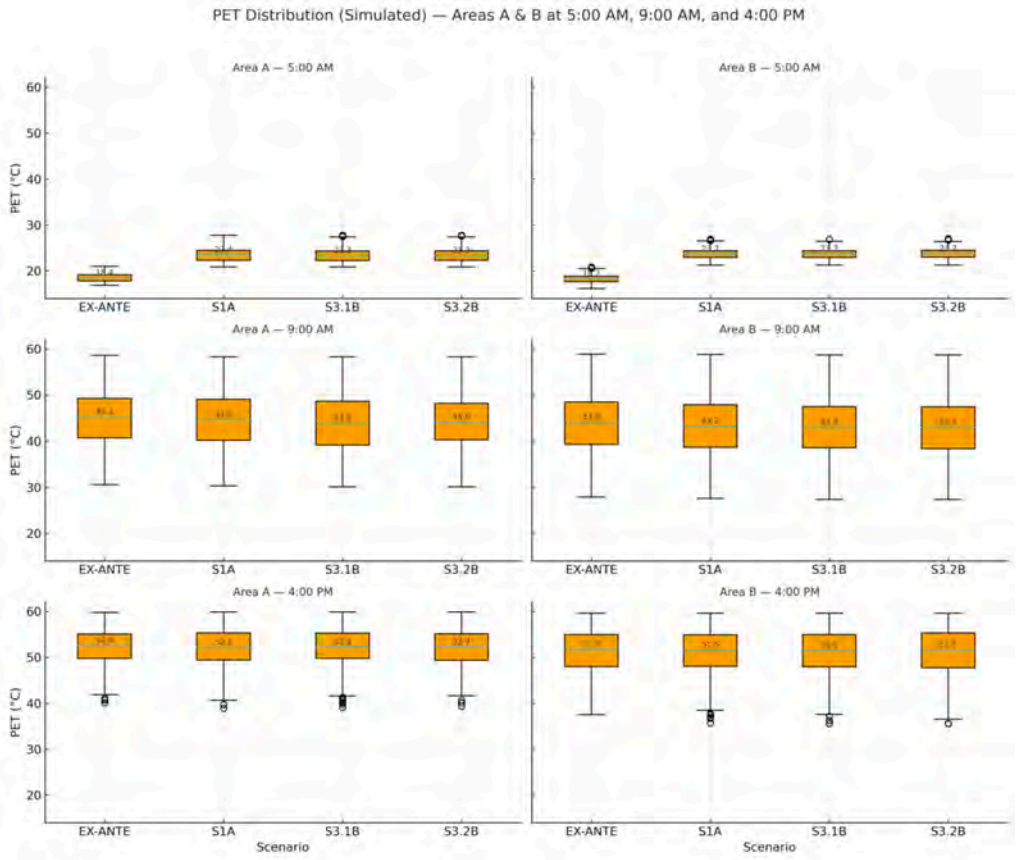

Figure 13. PET distribution for the surrounding areas (A and B) under selected greening scenarios at 5:00 a.m., 9:00 a.m., and 4:00 p.m. Boxplots represent the distribution of PET values, where the box indicates the interquartile range (IQR), the horizontal line inside the box represents the median, whiskers denote the data range, and circles indicate outliers.

At 4:00 p.m., differences among scenarios are smaller, with PET variations of approximately 0.1–0.2 °C.

At 5:00 a.m., PET values in the mitigation scenarios are slightly higher than in the ex-ante condition.

When comparing Area A and Area B, Area B exhibits lower PET values (0.4–0.8 °C) across all daytime scenarios.

Overall, greening interventions produce detectable but moderate daytime PET reductions in the surrounding areas, with the largest differences observed in the morning period.

4. Discussion

The discussion interprets the simulation results to clarify how vegetation density and spatial configuration influence thermal comfort across different times of day, land-use types, and spatial scales, with implications for climate-sensitive urban regeneration.

4.1. Temporal Performance of Greening Configurations

The results reveal a pronounced temporal dependency in the effectiveness of greening strategies. During the early-morning period (5:00 a.m.), PET values show negligible differences between mitigation scenarios and the ex-ante condition. This pattern suggests that vegetation configuration may have a limited influence on thermal comfort under nocturnal conditions. A possible explanation is that nighttime microclimatic processes are largely governed by longwave radiative exchanges and reduced solar forcing, during which evapotranspiration and shading effects are less pronounced [30,31]. However, the present study did not directly analyze radiative flux components; therefore, this interpretation should be considered indicative rather than conclusive.

At 9:00 a.m., clearer differences among greening scenarios emerge. The medium-density configuration (S2b) achieves the largest PET reduction within the regeneration area. This pattern may be associated with a balance between shading provision and air circulation under increasing solar radiation. Previous ENVI-met studies in Mediterranean contexts have reported that intermediate canopy densities can produce favorable thermal conditions during morning transition periods [25]. Nevertheless, diagnostic variables such as wind speed variation, mean radiant temperature (Tmrt), and latent heat flux were not explicitly isolated in this study; thus, the mechanisms underlying this performance should be interpreted as plausible rather than directly demonstrated.

Under peak afternoon conditions (4:00 p.m.), the distributed high-density configuration (S3.2b) provides the strongest PET mitigation. This outcome is likely related to enhanced shading and cumulative evapotranspiration under intense solar radiation. At the same time, the relatively limited spillover effects observed in surrounding areas may reflect reduced cooling efficiency with increasing distance from vegetated zones. Although afternoon moisture constraints could potentially influence evapotranspiration dynamics, the present simulations were conducted under default dry-summer soil moisture settings without explicit irrigation modelling. Therefore, any interpretation related to moisture limitation remains hypothetical and warrants further investigation through targeted analysis of soil moisture and surface energy balance components.

4.2. Zonal Variability and Land-Use Sensitivity

The zonal analysis reveals consistent PET differences among functional surface types. Across scenarios and time periods, mean PET values generally follow the order: public green areas < parking areas < building surroundings < path areas. This hierarchy indicates that surface characteristics and vegetation configuration strongly influence local thermal comfort.

Lower PET values in public green areas are likely related to combined shading and evapotranspiration effects provided by vegetation, which have been widely documented as key mechanisms of urban heat mitigation [27,28]. In contrast, path areas—characterized by linear geometry and higher exposure to direct solar radiation—consistently exhibit higher PET values, in line with findings from Mediterranean urban contexts [12,24].

Parking areas show intermediate performance, suggesting that tree shading can partially offset the thermal load of impervious surfaces. Building surroundings display slightly higher PET values, possibly reflecting geometric enclosure effects and variations in sky view factor, which are known to influence radiative exchange and airflow patterns [24,30].

Overall, the results suggest that the cooling performance of greening strategies depends not only on vegetation quantity but also on its spatial integration with specific land-use types.

4.3. Spatial Extent of Cooling Effects and Neighbourhood-Scale Implications

The analysis of adjacent areas (Areas A and B) indicates that the cooling benefits of greening interventions extend beyond the regeneration site, but their magnitude remains limited. Morning PET reductions of up to 0.6–0.8 °C were observed in surrounding zones, whereas afternoon differences were comparatively smaller.

This pattern suggests that vegetation-induced cooling attenuates with increasing distance from shaded and vegetated surfaces. Previous empirical and modelling studies have similarly reported that the thermal influence of urban green spaces decreases rapidly beyond their immediate boundaries, particularly under strong solar forcing [9,32]. The present findings are therefore consistent with established neighbourhood-scale microclimatic behaviour.

The weaker spillover effects observed during the afternoon peak may reflect the predominance of intense solar radiation and localized surface heating processes, under which cooling benefits become more confined to directly shaded areas. While variations in evapotranspiration efficiency under dry-summer conditions could potentially contribute to this attenuation, the simulations were conducted using default soil moisture settings without dynamic irrigation modelling. Consequently, interpretations related to moisture limitation remain indicative.

Differences between Areas A and B further suggest that background land-use composition and pre-existing vegetation may modulate the propagation of cooling effects. Urban microclimates at this scale are shaped by complex interactions among surface materials, morphology, and atmospheric processes [8,31]. However, disentangling these contributions would require dedicated diagnostic analysis beyond the scope of the present study.

Overall, the results indicate that the cooling benefits of greening strategies are primarily localized and dependent on vegetation density and spatial distribution. Rather than producing extensive spillover effects, effective urban heat mitigation may therefore rely on distributed and structurally integrated greening interventions across the urban fabric.

4.4. Model Considerations and Implications for Urban Design

The magnitude of PET reductions observed in this study is consistent with values reported in previous ENVI-met applications in Mediterranean and temperate climates, which typically range between 1 and 3 °C for daytime greening interventions [24,25]. This agreement supports the reliability of ENVI-met for comparative assessment of alternative greening strategies, particularly in early-stage urban design and planning contexts.

Nevertheless, the simulations are limited to a single extreme summer day and do not include site-specific field measurements for empirical validation. As such, the results should be interpreted as relative comparisons rather than absolute predictions. Despite these

limitations, the study provides robust insights into how vegetation density, structure, and spatial arrangement interact to shape microclimatic performance. Future research should integrate seasonal vegetation dynamics, multi-day simulations, and field measurements to further strengthen the empirical basis for climate-sensitive urban regeneration strategies. It is important to clarify that the present study does not implement a formal optimization framework based on objective functions or multi-objective trade-off analysis. Rather, the comparative scenario approach adopted here represents a design-oriented evaluation strategy aimed at identifying relatively higher-performing configurations under a worst-case summer condition.

Furthermore, although PET is widely recognized as a proxy indicator of human thermal stress and has established links with heat-related health risks in the literature, this study does not explicitly model exposure–risk chains or population-level vulnerability. Therefore, conclusions regarding resilience and health should be interpreted as indirect and design-supportive rather than as quantified epidemiological assessments.

5. Conclusions

This study evaluated the microclimatic effects of alternative greening configurations in an urban regeneration context using ENVI-met simulations. Results confirm that vegetation can effectively reduce thermal stress, although its performance is strongly dependent on time of day, vegetation density, and spatial arrangement.

No meaningful cooling effects were observed during the early-morning period, indicating a limited influence of greening under nocturnal conditions. In contrast, during the morning hours, medium-density vegetation achieved the highest cooling efficiency, producing PET reductions of up to approximately 2 °C within the intervention area and detectable but modest benefits in adjacent neighbourhoods. Under peak afternoon heat, distributed high-density configurations provided the strongest mitigation, highlighting the importance of both vegetation quantity and spatial layout.

The analysis also revealed pronounced differences among land-use types, with public green areas exhibiting the largest cooling effects, followed by parking, building, and path zones. Cooling benefits beyond the intervention site were found to be localized and limited in magnitude, underscoring the importance of widespread and distributed greening strategies rather than isolated interventions.

Overall, the findings emphasize the need to balance vegetation density, structure, and spatial distribution to maximize cooling performance in climate-sensitive urban regeneration projects. Future research should explore seasonal vegetation dynamics, multi-day simulations, and integrated design optimization approaches to further support urban heat mitigation strategies. The simulation framework adopted in this study was intentionally based on a representative extreme summer day, corresponding to the highest heat index recorded during the reference year. This approach enables the evaluation of greening performance under critical thermal stress conditions and functions as a climatic stress-test for alternative design configurations. By focusing on a worst-case scenario, the analysis highlights the relative effectiveness of vegetation density and spatial arrangement in mitigating peak heat exposure at pedestrian level.

At the same time, the findings should be interpreted as context-specific design insights for climate-responsive urban regeneration rather than as universally transferable prescriptions. The results demonstrate how vegetation structure and spatial distribution influence microclimatic performance within a defined urban morphology and meteorological condition, offering a structured scenario-based framework that can inform similar analyses in other contexts.

Extending the simulations to average seasonal conditions and multiple representative meteorological scenarios would provide a more comprehensive assessment of greening effectiveness across different climatic situations. Future research should therefore incorporate multi-day and multi-season modeling approaches to evaluate the robustness, stability, and potential trade-offs of vegetation configurations under both typical and extreme weather conditions.

Such developments would further strengthen the applied and transferable relevance of scenario-based microclimatic design assessment. In this perspective, interdisciplinary collaboration among architecture, urban planning, and agricultural engineering disciplines may foster more integrated strategies for the planning and management of peri-urban and consolidated urban areas, where green infrastructure plays a central role in shaping environmental quality, thermal comfort, and long-term urban resilience.

Author Contributions: Z.Z.: Conceptualization, Methodology, Formal Analysis, Investigation, Data curation, Visualization, Writing—Original Draft; A.B.: Conceptualization, Methodology, Data curation, Writing—Original Draft; L.C.: Investigation, Data curation, Visualization, Writing—review & editing; P.T.: Conceptualization, Supervision, Resources, Writing—review & editing, Project administration, Resources; D.T.: Conceptualization, Methodology, Investigation, Resources, Supervision, Project administration, Writing—Original Draft, Writing—review & editing, Resources. All authors have read and agreed to the published version of the manuscript.

Funding: This work was funded by the European Union under the Marie Skłodowska-Curie Actions Doctoral Networks (MSCA-DN) programme through the GreeNexUS project (Grant Agreement No. 101073437). The views and opinions expressed are those of the authors only and do not necessarily reflect those of the European Union or the granting authority.

Data Availability Statement: The data presented in this study are available on reasonable request from the corresponding author. The simulation input files and model configurations can be provided upon request.

Acknowledgments: The authors would like to thank the Municipality of Imola for the kind collaboration in providing base maps and materials about the study area, information about the city's sustainability strategies, and Area Blu for providing the georeferenced tree inventory.

Conflicts of Interest: The authors declare no conflict of interest.

Abbreviations

HI	Heat Index
CEST	Central European Summer Time
T_a	Air Temperature
RH	Relative Humidity
WS	Wind Speed
WD	Wind Direction
PET	Physiological Equivalent Temperature (°C)
UTCI	Universal Thermal Climate Index
PMV	Predicted Mean Vote
PDD	Predicted Percentage Dissatisfied (%)
UHI	Urban Heat Island
NBSs	Nature-Based Solutions
ENVI-met	Environmental Microclimate Simulation Software

References

1. Lee, H.; Calvin, K.; Dasgupta, D.; Krinner, G.; Mukherji, A.; Thorne, P.; Trisos, C.; Romero, J.; Aldunce, P.; Barrett, K.; et al. *IPCC, 2023: Climate Change 2023: Synthesis Report: A Report of the Intergovernmental Panel on Climate Change*; Intergovernmental Panel on Climate Change: Geneva, Switzerland, 2023. [CrossRef]
2. Arrar, H.F.; Kaoula, D.; Santamouris, M.; Foufa-Abdessemed, A.; Emmanuel, R.; Matallah, M.E.; Ahriz, A.; Attia, S. Coupling of different nature base solutions for pedestrian thermal comfort in a Mediterranean climate. *Build. Environ.* **2024**, *256*, 111480. [CrossRef]
3. Murray, J.; Heggie, D. From urban to national heat island: The effect of anthropogenic heat output on climate change in high population industrial countries. *Earths Future* **2016**, *4*, 298–304. [CrossRef]
4. Akbari, H.; Kolokotsa, D. Three decades of urban heat islands and mitigation technologies research. *Energy Build.* **2016**, *133*, 834–842. [CrossRef]
5. Yasobant, S.; Lekha, K.S.; Trivedi, P.; Krishnan, S.; Kator, C.; Kaur, H.; Adaniya, M.; Sinha, A.; Saxena, D. Impact of heat on human and animal health in India: A landscape review. *Dialogues Health* **2025**, *6*, 100203. [CrossRef] [PubMed]
6. Gaspari, J.; Fabbri, K.; Lucchi, M. The use of outdoor microclimate analysis to support decision making process: Case study of Bufalini square in Cesena. *Sustain. Cities Soc.* **2018**, *42*, 206–215. [CrossRef]
7. Gholami, M.; Barbaresi, A.; Tassinari, P.; Bovo, M.; Torreggiani, D. A Comparison of Energy and Thermal Performance of Rooftop Greenhouses and Green Roofs in Mediterranean Climate: A Hygrothermal Assessment in WUFI. *Energies* **2020**, *13*, 2030. [CrossRef]
8. Saaroni, H.; Amorim, J.H.; Hiemstra, J.A.; Pearlmutter, D. Urban Green Infrastructure as a tool for urban heat mitigation: Survey of research methodologies and findings across different climatic regions. *Urban Clim.* **2018**, *24*, 94–110. [CrossRef]
9. Oliveira, S.; Andrade, H.; Vaz, T. The cooling effect of green spaces as a contribution to the mitigation of urban heat: A case study in Lisbon. *Build. Environ.* **2011**, *46*, 2186–2194. [CrossRef]
10. Noro, M.; Lazzarin, R. Urban heat island in Padua, Italy: Simulation analysis and mitigation strategies. *Urban Clim.* **2015**, *14*, 187–196. [CrossRef]
11. Knaus, M.; Haase, D. Green roof effects on daytime heat in a prefabricated residential neighbourhood in Berlin, Germany. *Urban For. Urban Green.* **2020**, *53*, 126738. [CrossRef]
12. Aboelata, A. Reducing outdoor air temperature, improving thermal comfort, and saving buildings' cooling energy demand in arid cities—Cool paving utilization. *Sustain. Cities Soc.* **2021**, *68*, 102762. [CrossRef]
13. Di Marino, M.; Tiitu, M.; Saglie, I.-L.; Lapintie, K. Conceptualizing 'green' in urban and regional planning—The cases of Oslo and Helsinki. *Eur. Plan. Stud.* **2024**, *32*, 1187–1209. [CrossRef]
14. Delshammar, T. Urban Greening Strategies for Compact Areas—Case Study of Malmö, Sweden. *Nord. Arkit.* **2014**, *26*. Available online: https://arkitekturforskning.net/na/article/view/499 (accessed on 5 March 2026).
15. Russo, A.; Cirella, G.T. Modern Compact Cities: How Much Greenery Do We Need? *Int. J. Environ. Res. Public Health* **2018**, *15*, 2180. [CrossRef]
16. Aslanoğlu, R.; Kazak, J.K.; Szewrański, S.; Świąder, M.; Arciniegas, G.; Chrobak, G.; Jakóbiak, A.; Turhan, E. Ten questions concerning the role of urban greenery in shaping the future of urban areas. *Build. Environ.* **2025**, *267*, 112154. [CrossRef]
17. Davies, C.; Lafortezza, R. Urban green infrastructure in Europe: Is greenspace planning and policy compliant? *Land Use Policy* **2017**, *69*, 93–101. [CrossRef]
18. Peel, M.C.; Finlayson, B.L.; McMahon, T.A. Updated world map of the Köppen-Geiger climate classification. *Hydrol. Earth Syst. Sci.* **2007**, *11*, 1633–1644. [CrossRef]
19. World Meteorological Organization. WMO Climatological Normals. Available online: https://community.wmo.int/site/knowledge-hub/programmes-and-initiatives/climate-services/wmo-climatological-normals (accessed on 27 February 2026).
20. Commue di Imola. La Giunta ha Approvato la Variante 3 al Piano Particolareggiato di Iniziativa Pubblica N8 Nord Ferrovia. Available online: https://www.comune.imola.bo.it/novita/comunicati/2023/12/la-giunta-ha-approvato-la-variante-3-al-piano-particolareggiato-di-iniziativa-pubblica-n8-nord-ferrovia (accessed on 17 January 2025).
21. Emilia-Romagna Region. Soil Maps in Emilia-Romagna Region. Available online: https://ambiente.regione.emilia-romagna.it/en/geologia/soil/soil-knowledge/carte-dei-suoli-emilia-romagna (accessed on 17 January 2025).
22. Bruse, M.; Fleer, H. Simulating surface–plant–air interactions inside urban environments with a three dimensional numerical model. *Environ. Model. Softw.* **1998**, *13*, 373–384. [CrossRef]
23. Yang, X.; Zhao, L.; Bruse, M.; Meng, Q. Evaluation of a microclimate model for predicting the thermal behavior of different ground surfaces. *Build. Environ.* **2013**, *60*, 93–104. [CrossRef]
24. Tsoka, S.; Tsikaloudaki, A.; Theodosiou, T. Analyzing the ENVI-met microclimate model's performance and assessing cool materials and urban vegetation applications—A review. *Sustain. Cities Soc.* **2018**, *43*, 55–76. [CrossRef]
25. Salata, F.; Golasi, I.; de Lieto Vollaro, R.; de Lieto Vollaro, A. Urban microclimate and outdoor thermal comfort. A proper procedure to fit ENVI-met simulation outputs to experimental data. *Sustain. Cities Soc.* **2016**, *26*, 318–343. [CrossRef]

26. Ronchi, S.; Arcidiacono, A.; Pogliani, L. Integrating green infrastructure into spatial planning regulations to improve the performance of urban ecosystems. Insights from an Italian case study. *Sustain. Cities Soc.* **2020**, *53*, 101907. [CrossRef]
27. Bowler, D.E.; Buyung-Ali, L.; Knight, T.M.; Pullin, A.S. Urban greening to cool towns and cities: A systematic review of the empirical evidence. *Landsc. Urban Plan.* **2010**, *97*, 147–155. [CrossRef]
28. Shashua-Bar, L.; Hoffman, M.E. Geometry and orientation aspects in passive cooling of canyon streets with trees. *Energy Build.* **2003**, *35*, 61–68. [CrossRef]
29. Matzarakis, A.; Mayer, H.; Iziomon, M.G. Applications of a universal thermal index: Physiological equivalent temperature. *Int. J. Biometeorol.* **1999**, *43*, 76–84. [CrossRef]
30. Anderson, G.B.; Bell, M.L.; Peng, R.D. Methods to Calculate the Heat Index as an Exposure Metric in Environmental Health Research. *Environ. Health Perspect.* **2013**, *121*, 1111–1119. [CrossRef]
31. Oke, T.R. The energetic basis of the urban heat island. *Q. J. R. Meteorol. Soc.* **1982**, *108*, 1–24. [CrossRef]
32. Zardo, L.; Geneletti, D.; Pérez-Soba, M.; Van Eupen, M. Estimating the cooling capacity of green infrastructures to support urban planning. *Ecosyst. Serv.* **2017**, *26*, 225–235. [CrossRef]